



Received: 5 March 2018

DOI: 10.1002/mop.31373

# Rectangular dielectric resonator antenna fed by offset tapered copper and graphene microstrip lines for 5G communications

Wei Xia | Bohan Zhang |  
Wenqing Zhou | Jingwei Zhang |  
Chengguo Liu | Daping He |  
Zhi Peng Wu

Hubei Engineering Research Center of RF-Microwave Technology and Application, School of Science, Wuhan University of Technology, Wuhan, China

## Correspondence

Zhi Peng Wu  
Email: z.p.wu@whut.edu.cn

## Abstract

In this paper, rectangular dielectric resonator antennas (RDRAs) fed by offset tapered copper and graphene microstrip lines are presented. A comparison between these two feeding materials is made with an aim of using the high-conductivity graphene film (HCGF) to replace copper for feeding the RDRA if feasible. Four feed forms have been discussed. The presented feed mechanism is able to couple electromagnetic energy in three different modes of the RDRA. The HCGF is utilized to replace copper for feeding the RDRA. An impedance bandwidth of 11.32% (3.25 GHz ~ 3.64 GHz) is realized in the experiments by using a graphene feed line, compared to that of 12.24% (3.22 GHz ~ 3.64 GHz) for copper, and a peak gain of 4.48dBi is obtained at the center frequency. The results show that the HCGF can be used to couple the RDRA, and the HCGF fed RDRA has good performance. Radiation patterns around the center frequency are also presented.

## KEYWORDS

5G communications, dielectric resonator antennas, graphene, tapered microstrip line

## 1 | INTRODUCTION

With the increasing popularity of intelligent terminals and data stream, the fourth-generation mobile communication

network has not been able to satisfy people's demand on the network in capacity, rate, and frequency spectrum.<sup>1</sup> The technological developments of the fifth-generation (5G) mobile communication network will therefore be the focus for the next few years. Among all the allocated frequencies for 5G applications, 3.5GHz (3.3GHz~3.6GHz) is the band that probably will be firstly deployed for the wireless communications.<sup>2</sup> As an indispensable part of the communication system, antenna is a key component to meet 5G application requirements. Multiple-input multiple-output (MIMO) antennas have been reported for 3.5GHz band communication.<sup>3,4</sup> However, the efficiencies of these metal-based printed MIMO antennas are relatively low (under 65%), and the configurations are relatively complex.<sup>5</sup>

Due to their high radiation efficiency, low loss, broad bandwidth, compact size, flexible and diverse feed mechanism, dielectric resonators has been extensively studied in the past two decades. Various feed mechanisms can be used to excite the radiating modes of the dielectric resonator antennas (DRAs), including the use of a coaxial probe, microstrip line, slot coplanar waveguide.<sup>6</sup> However, different feed mechanisms may result in different impedance bandwidth. Among them, microstrip line is a simple and convenient feed method to use. Compared to the 50  $\Omega$  standard microstrip line, the use of a tapered microstrip line can effectively increase the impedance bandwidth of DRA.<sup>7</sup> Moreover, DRAs with offset-fed can generate multiple modes and broaden the impedance bandwidth.<sup>8</sup>

On one hand, RF and microwave antennas need to meet new requirements, such as smaller size, lighter weight, higher efficiency, lower loss, rapid heat transfer, and cost. Traditional metal antennas could not achieve all of these requirements at one time. On the other hand, graphene-based antennas could provide new features in RF devices. Graphene, either in its single layer and multi-layer form, has a lot of unique properties like high conductivity of 6000 S/cm and extreme high thermal conductivity of 5000  $\text{W}\cdot\text{m}^{-1}\cdot\text{K}^{-1}$ , which is very suitable for RF antenna design.<sup>9,10</sup> As far as we know, most investigations of graphene-based antennas are focused in THz band.<sup>11-13</sup> A novel and simple dielectric grating-based graphene leaky-wave antenna of reconfigurable radiation pattern is reported by J. Li.<sup>11</sup> A waveguide-fed tunable terahertz graphene antenna with high radiation efficiency is presented by S. E. Hosseini and N. Komjani.<sup>12</sup> This antenna is likely to be employed for various radiated-wave applications such as wireless communication in electromagnetic nanonetworks and sensing. W. Fuscaldo et al. have analyzed the dissipation losses in plasmonic graphene-based THz antennas.<sup>13</sup> Above studies give the feasibility of graphene based antenna in THz band. Moreover, in mobile communication frequency band, a graphene-flakes-based screen-printed wideband elliptical dipole antenna is reported for low-cost wireless communications applications in the work of A. Lamminen.<sup>14</sup> The

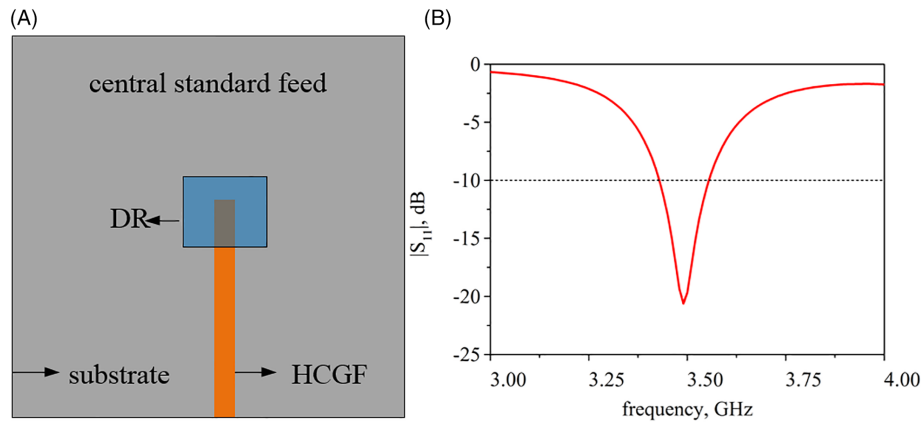


**FIGURE 1** The traditional RDRA fed by central standard HCGF microstrip line. A, Feed structure; B, the simulated  $|S_{11}|$  response [Color figure can be viewed at [wileyonlinelibrary.com](http://wileyonlinelibrary.com)]

performance of using graphene in frequency reconfigurable antennas of two hybrid metal-graphene antennas for WIFI and LTE applications has also been analyzed.<sup>15</sup> However, RDRA with graphene feed have not yet been studied. The graphene materials will endow the RDRA with new features due to their properties of high conductivity, high thermal conversion efficiency in high-power transmission, and stabilization in complicated environment. Though the investigation is in low power, the proposed antenna has more advantages in high-power transmission.

In this paper, a novel approach to the design of a 3.5 GHz broadband RDRA based on a tapered graphene feed is presented. The graphene film has a high conductivity of  $1.1 \times 10^6$  S/m. The tapered graphene feed line with one end widened is coupled with the rectangular dielectric resonator with only one side edge attaching to the RDRA. The tapered graphene fed RDRA is simulated, tested, and compared with that of copper feed. The simulated and measured results for both graphene and copper feeds are reported in this paper.

This paper is organized in four sections. In Section 2, the design, simulated results, and parameters of a tapered microstrip-fed RDRA will be presented. The RDRA with four feed structures will be described. The technique of

asymmetrical offset feed mechanism, which excites three modes will be presented. In Section 3, RDRA with tapered copper and graphene microstrip lines will be compared. Both measured results with four different feed forms will be presented, including return loss, radiation patterns and gain will be presented. Conclusions will be drawn in Section 4.

## 2 | ANTENNA DESIGN AND SIMULATIONS

The dielectric resonator (DR) is placed above a RT5880 substrate. The relative permittivity of rectangular RDRA is  $\epsilon_r = 37$ . The dimensions of rectangular RDRA are  $l = 14.5$  mm,  $w = 14.5$  mm and  $h = 7$  mm for the length, width, and height, respectively. For the analysis of an RDRA, Marcanti has proposed a dielectric waveguide model to estimate the resonant frequency and Q-factor of the RDRA.<sup>16</sup> Zhang, B.H. has then simplified the procedures for calculating the resonant frequency of  $TE_{111}^y$  mode of an RDRA placed above a dielectric substrate.<sup>8</sup> The resonant frequency of  $TE_{111}^y$  mode of RDRA can therefore be calculated by using the following formulas:

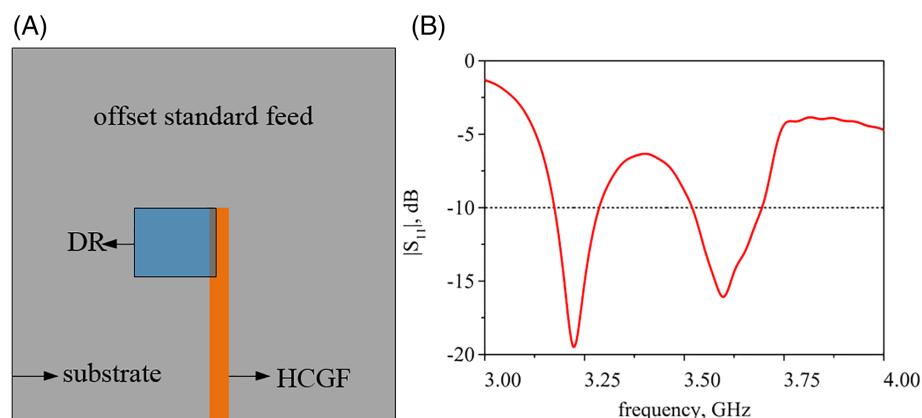


**FIGURE 2** The RDRA fed by offset standard HCGF microstrip line. A, Feed structure; B, the simulated  $|S_{11}|$  response [Color figure can be viewed at [wileyonlinelibrary.com](http://wileyonlinelibrary.com)]

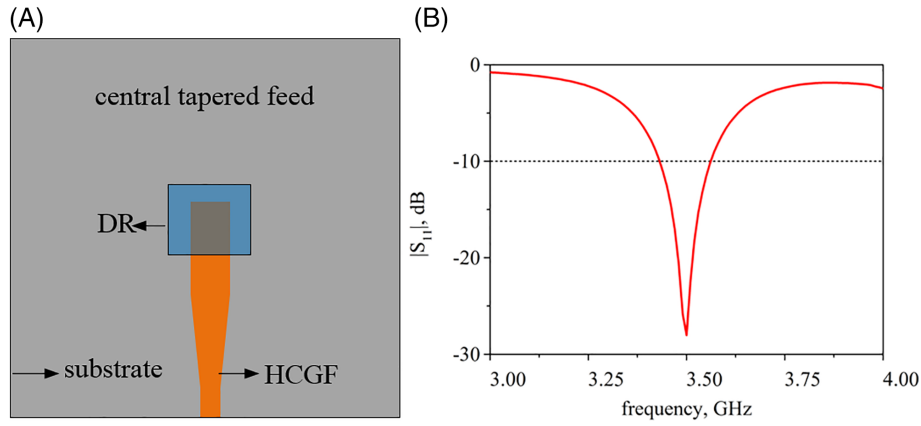


**FIGURE 3** The RDRA fed by central tapered HCGF microstrip line. A, Feed structure; B, the simulated  $|S_{11}|$  response [Color figure can be viewed at wileyonlinelibrary.com]

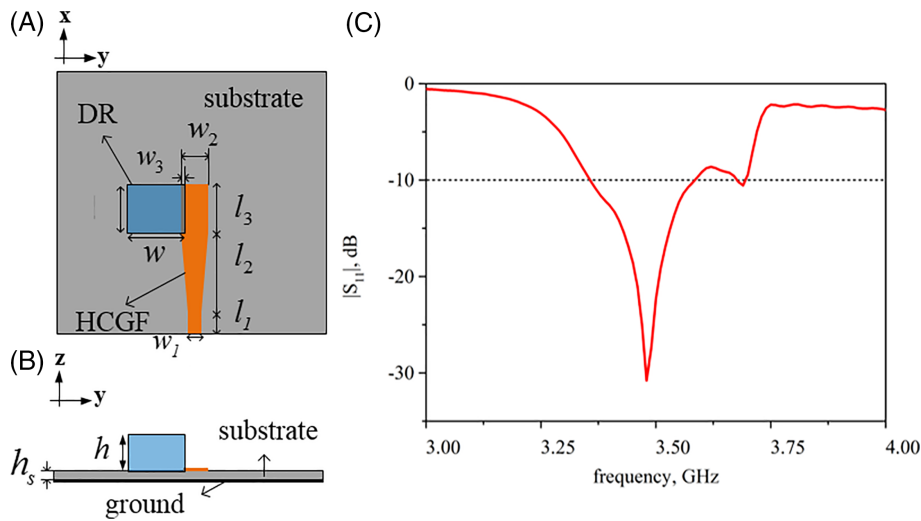


**FIGURE 4** The RDRA fed by offset tapered HCGF microstrip line. A, The top view of feed structure; B, the side view of feed structure. C, The simulated  $|S_{11}|$  response [Color figure can be viewed at wileyonlinelibrary.com]

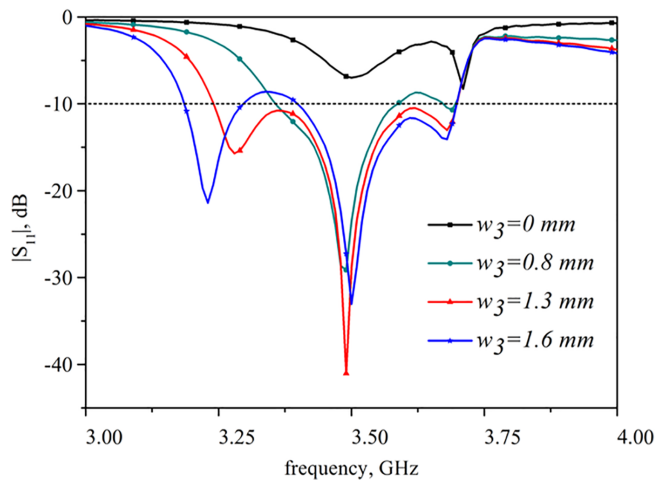


**FIGURE 5** Simulated  $|S_{11}|$  response for different  $w_3$  [Color figure can be viewed at wileyonlinelibrary.com]

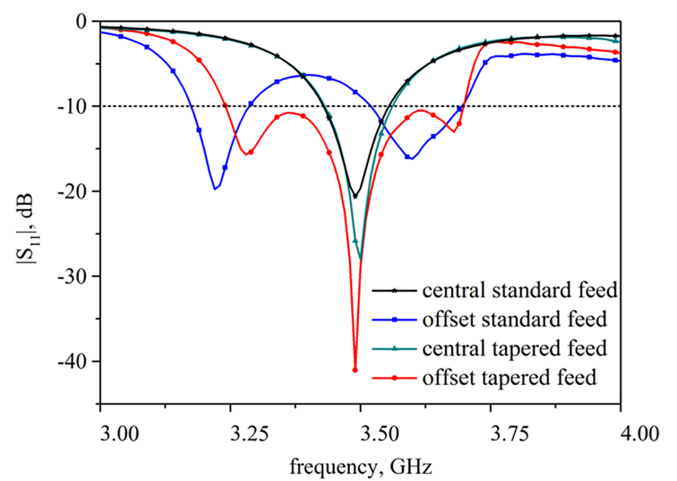


**FIGURE 6** The simulated results of  $|S_{11}|$  for four feed forms [Color figure can be viewed at wileyonlinelibrary.com]

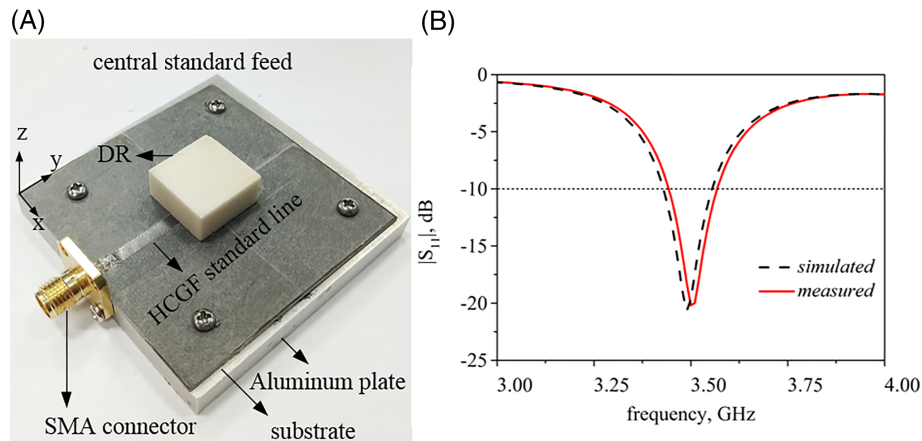


**FIGURE 7** The fabrication and measurement of RDRA with central standard line. A, The prototype of the RDRA; B, the measured and simulated  $|S_{11}|$  response [Color figure can be viewed at [wileyonlinelibrary.com](http://wileyonlinelibrary.com)]

$$k_x = \pi/l \quad (1)$$

$$k_y \tan(k_y w/2) = \sqrt{(\epsilon_r - 1)k_0^2 - k_y^2} \quad (2)$$

$$k_z h = \pi/2 + \alpha \quad (3)$$

$$\tan \alpha = \sqrt{\epsilon_r/\epsilon_s} \tan(k_0 \sqrt{\epsilon_s} h_s) \quad (4)$$

$$k_x^2 + k_y^2 + k_z^2 = \epsilon_r k_0^2 \quad (5)$$

$$f_r = \frac{k_0 c}{2\pi} \quad (6)$$

where  $k_0$  is the wave number in free space,  $k_x$ ,  $k_y$ , and  $k_z$  are wave numbers in  $X$ ,  $Y$ , and  $Z$  directions respectively,  $c$  is the speed of light in free space,  $\epsilon_s$  is the relative dielectric constant of the substrate and  $h_s$  thickness of the substrate. The resonant frequency of calculation result is  $f_r = 3.511$  GHz.

Firstly, the traditional central standard feed is utilized to feed RDRA. The feed structure is shown in Figure 1A,B shows the simulated  $|S_{11}|$  response. It can be observed that the  $-10$  dB impedance bandwidths is only 3.73% (3.42 GHz  $\sim$  3.55 GHz), and just the fundamental mode ( $TE_{111}^y$  mode) is excited. The feed form needs to be improved.

## 2.1 | RDRA with offset standard feed line

In order to increase the resonance modes of RDRA, the RDRA is placed asymmetrically. The feed structure is shown in Figure 2A,B shows the simulated  $|S_{11}|$  response. Two modes ( $TE_{111}^x$ ,  $TE_{111}^y$  modes) are excited, but separated modes are unable to provide continuous  $-10$  dB impedance bandwidth (3.18 GHz  $\sim$  3.28 GHz, 3.53  $\sim$  3.69 GHz). The shape of feed line needs to be changed.

## 2.2 | RDRA with central tapered feed line

A tapered HCGF microstrip line is used to feed the RDRA. The feed structure is shown in Figure 3A,B shows the simulated  $|S_{11}|$  response. The  $-10$  dB impedance bandwidth is still narrow with 3.43% (3.44 GHz  $\sim$  3.56 GHz).

## 2.3 | RDRA with offset tapered feed line

The geometry of proposed antenna is shown in Figure 4A,B. The substrate has a relative permittivity of 2.2 and thickness  $h_s = 0.787$  mm. The tapered microstrip line consists of a standard  $50 \Omega$  microstrip line section ( $w_1 = 2.4$  mm,  $l_1 = 6$  mm), a

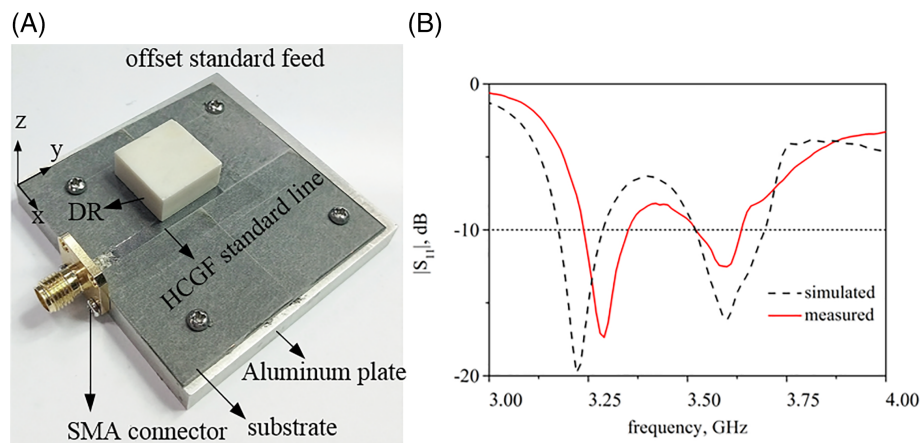


**FIGURE 8** The fabrication and measurement of RDRA with offset standard line. A, The prototype of the RDRA; B, the measured and simulated  $|S_{11}|$  response [Color figure can be viewed at [wileyonlinelibrary.com](http://wileyonlinelibrary.com)]



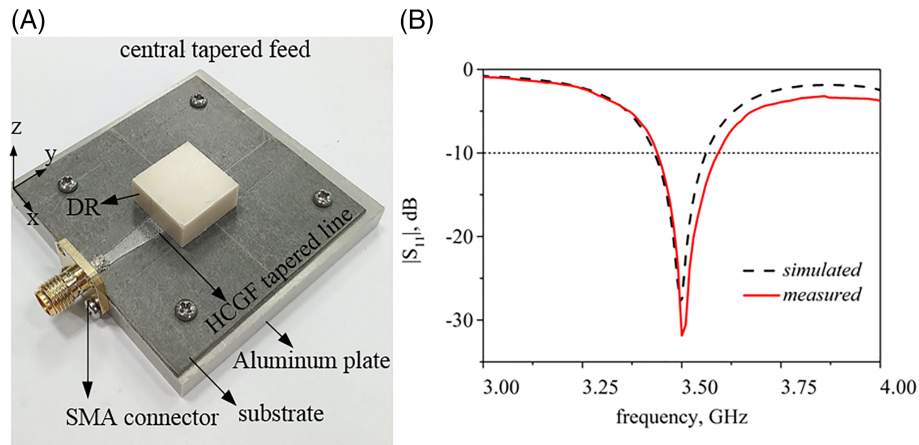


**FIGURE 9** The fabrication and measurement of RDRA with central tapered line. A, The prototype of the RDRA; B, the measured and simulated  $|S_{11}|$  response [Color figure can be viewed at wileyonlinelibrary.com]

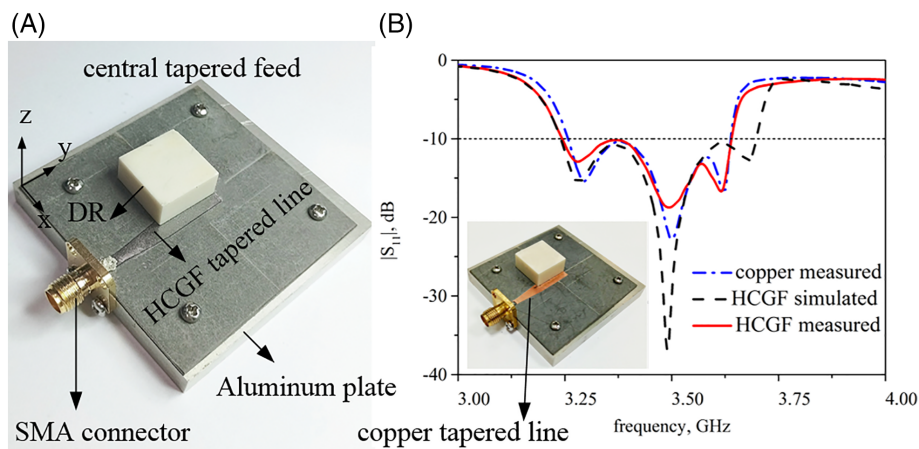


**FIGURE 10** The fabrication and measurement of RDRA with offset tapered line. A, The prototype of the RDRA fed by HCGF; B, the measured and simulated  $|S_{11}|$  response [Color figure can be viewed at wileyonlinelibrary.com]

tapered microstrip line section ( $l_2 = 10$  mm) and  $30 \Omega$  microstrip line section ( $w_2 = 4.5$  mm, initial  $w_3 = 0.8$  mm  $l_3 = 14.5$  mm approximate  $\lambda/4$  length). An SMA connector is connected to the  $50 \Omega$  microstrip line section. The RDRA is at the edge of  $30 \Omega$  microstrip line. Unlike the conventional approaches of feeding a RDRA with a microstrip line placed at the centre of the RDRA, this method is to feed the RDRA with the antenna covering only one edge of the microstrip line with an overlapping width  $w_3$ . The Figure 4C shows the simulated  $|S_{11}|$  response, where three modes ( $TE_{111}^x$ ,  $TE_{111}^y$  and a third adjacent mode) of resonance can be observed, and the parameters of RDRA need to be optimized.

The dimensions and dielectric parameters of RDRA mentioned above are implemented in the simulation. Microstrip line width  $w_2$  and the overlapping width  $w_3$  are key parameters to control the coupling. The value of  $w_2$  is optimized to adjust the antenna operation frequency to 3.5GHz with sufficient bandwidth. There is a shift in resonance frequency as  $w_2$  increases. In order to obtain impedance bandwidth as wide as possible,  $w_2 = 4.5$  mm is set as an optimum chosen value. The simulated results of  $|S_{11}|$  for different  $w_3$  values in the range between 0 to

1.6 mm are shown in Figure 5. With the increase of  $w_3$ , the impedance bandwidth becomes wider. But when  $w_3 = 1.6$  mm, some part of the curve between two  $|S_{11}|$  dips is above  $-10$  dB. Hence,  $w_3 = 1.3$  mm is chosen in the design, which

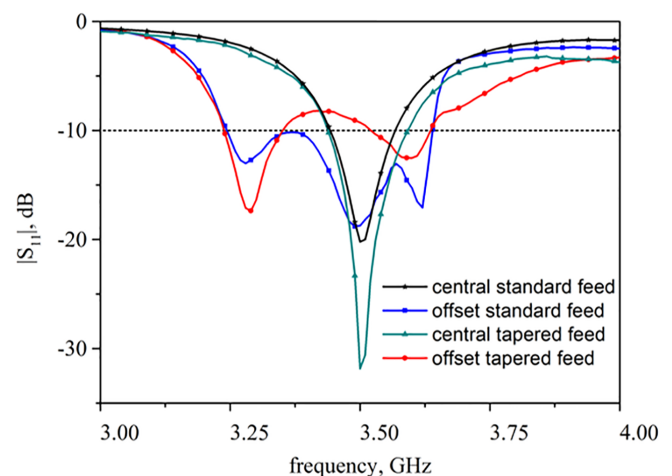


**FIGURE 11** The measured results of  $|S_{11}|$  for four feed forms [Color figure can be viewed at wileyonlinelibrary.com]

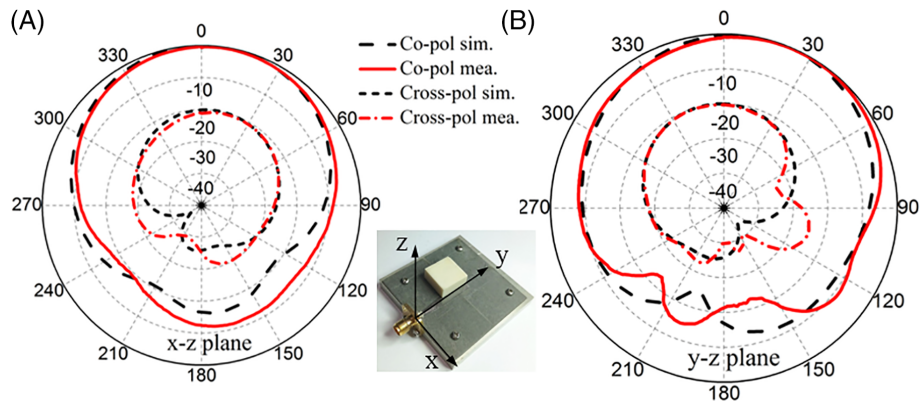


**FIGURE 12** Normalized simulated and measured radiation patterns; A,  $x$ - $z$  plane; B,  $y$ - $z$  plane [Color figure can be viewed at [wileyonlinelibrary.com](http://wileyonlinelibrary.com)]

leads to a wide  $-10$  dB impedance bandwidth of 13.26% (3.24 GHz  $\sim$  3.70 GHz) in the simulation.

In addition, the simulated results of the RDRA fed by four different feed forms are shown in Figure 6. Compared with the  $50\ \Omega$  standard offset feed line, the offset-feed with a tapered microstrip line can significantly increase the bandwidth of the antenna, and the  $-10$  dB impedance bandwidth is increased from 3.43% (3.44 GHz  $\sim$  3.56GHz) to 13.26% (3.24 GHz  $\sim$  3.70 GHz). The number of coupled antenna resonant modes changes from one mode to three modes. Compared with the symmetrical feed mechanism, the use of an asymmetrically offset-fed line can also increase bandwidth, and the  $-10$  dB impedance bandwidth is increased by 3.87 times. The offset-fed tapered line is therefore an optimum selection when considering bandwidth enhancement.

### 3 | HCGF FED RDRA FABRICATION AND MEASURED RESULTS

The HCGF microstrip line structure above is fabricated from a sheet of HCGF with conductivity  $\sigma = 1.1 \times 10^6$  S/m using laser engraving technique. The HCGF tapered microstrip line is taped on the substrate with conductive silver glue, and the substrate is fixed to the aluminum plate with four screws. Next, RDRA fed by different feed structure will be fabricated and measured.

#### 3.1 | RDRA fabricated with standard line

With the substrate and SMA connectors in place, the HCGF fed RDRA with central standard microstrip line is shown in Figure 7A,B shows the simulated and measured  $|S_{11}|$  response. It can be observed that the measured results are very similar with the simulated results. The HCGF-fed RDRA with offset standard microstrip line fabricated by moving the DR is shown in Figure 8A,B shows the simulated and measured  $|S_{11}|$  response. The measured result of  $-10$  dB impedance bandwidth is lightly narrower than the simulated bandwidth, but it still has two resonant modes and can be improved.

The good agreements between the simulation and measurement demonstrates that the HCGF is able to couple with the RDRA.

#### 3.2 | RDRA fabricated with central tapered line

The HCGF fed RDRA with central tapered microstrip line is shown in Figure 9A,B shows the simulated and measured  $|S_{11}|$  response. Similar results prove the feasibility of the HCGF fed RDRA once again.

#### 3.3 | RDRA fabricated with offset tapered line

The RDRA fed by tapered microstrip line is shown in Figure 10. Figure 10A shows the HCGF-fed RDRA with offset tapered microstrip line, as compared to a counterpart made from copper in Figure 10B. The fabricated HCGF and copper-fed RDRA are measured with a Network Analyzer (PNA, Keysight N5247A). The measured results of  $|S_{11}|$  responses are compared in Figure 10B. The results show that there is a good agreement between the copper and HCGF fed RDRA, but the HCGF fed RDRA has a lightly wider bandwidth (3.25 GHz - 3.64 GHz). It can be observed that

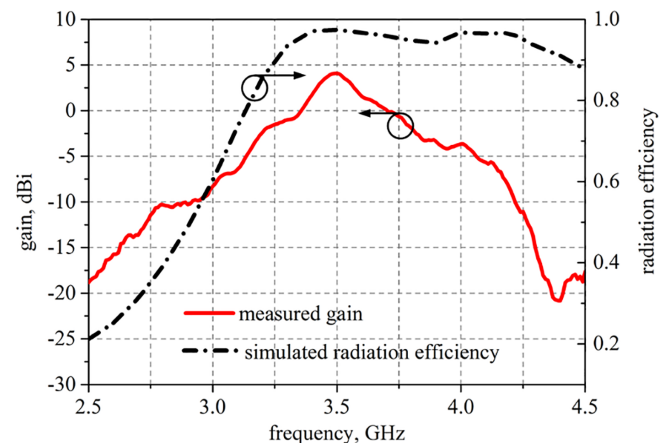


**FIGURE 13** Measured gain and simulated radiation efficiency [Color figure can be viewed at [wileyonlinelibrary.com](http://wileyonlinelibrary.com)]

the maximal  $|S_{11}|$  of the HCGF RDRA is smaller 4.19 dB than the copper-fed RDRA, which is probably caused by the air gap between the graphene films and substrate. The proposed HCGF-fed antenna shows similar performance to the metal antenna. In addition, the lower cost and lighter weight of graphene antenna are good candidate.

In order to prove the advantage of offset tapered feed, four feed forms discussed previously of RDRA are measured. The measured results of  $|S_{11}|$  responses are shown in Figure 11. Compared to the simulated results in Figure 6, the simulated results are better than the measured results, which may be due to the coarse surface of the rectangular dielectric resonator, the losses of connectors, and cables. However, the overall trend of all curves is consistent. The measured impedance bandwidth is 2.21% lower than the simulated bandwidth, but it is still able to cover the 3.5GHz band (3.3 GHz – 3.6 GHz).

In addition to the  $|S_{11}|$  and bandwidth, the gain and the radiation pattern are also very important factors for the antenna performance. The radiation patterns of HCGF fed RDRA at resonant frequency are measured in the microwave anechoic chamber. The simulated and measured far-field radiation patterns at 3.5GHz on  $x$ - $z$  plane and  $y$ - $z$  plane are shown in Figure 12A,B. The antenna radiates at the broadside direction, which is expected for the  $TE_{111}^x$ ,  $TE_{111}^y$ , and a third adjacent mode of RDRA. It is seen that the results of measurement and simulation agree very well. On the  $x$ - $z$  plane, the radiation pattern is almost symmetrical in the operating frequency range. As can be observed from the Figure 12, the maximum radiation on the  $y$ - $z$  plane deviates from the  $-x$  axis by 30° due to the asymmetry of the RDRA placement. The cross-polar radiation is –20 dB lower than the co-polar radiation. Figure 13 shows the measured antenna gain and simulated radiation efficiency. The largest gain in measurement is 4.48dBi at operating frequency, and the maximum of simulated radiation efficiency can achieve 97.4%.

## 4 | CONCLUSIONS

In summary, a RDRA offset-fed by a HCGF-tapered microstrip line has been investigated and tested. The microstrip width  $w_2$  and overlapping width  $w_3$  are demonstrated to be effective in increasing coupling and enlarging impedance bandwidth. The proposed antenna covers 3.25 GHz ~ 3.64 GHz, where the radiation patterns of measured and simulated results are in good agreement. In addition, the peak gain is 4.48dBi with high radiation efficiency (97.4%). The results demonstrate that the high-conductivity graphene film can be used to replace the copper for feeding the RDRA, and the low conductivity graphene film probably influences the antenna performance. The proposed RDRA has novel material, compact size, simple feed structure, and sufficient bandwidth for 5G applications.

## ORCID

Jingwei Zhang  <http://orcid.org/0000-0003-0657-6193>

Daping He  <http://orcid.org/0000-0002-0284-4990>

Zhi Peng Wu  <http://orcid.org/0000-0002-4879-3279>

## REFERENCES

- [1] Gupta A, Jha RK. A survey of 5G network: architecture and emerging technologies. *IEEE Access*. 2015;3:1206-1232.
- [2] China Mobile Communications Corporation, Guideline for 3.5GHz 5G System Prototype and Trial, Mobile World Congress (MWC), Barcelona, Spain, 2017.
- [3] Wong KL, Lu JY, Chen LY, Li WY, Ban YL. 8-antenna and 16-antenna arrays using the quad-antenna linear array as a building block for the 3.5 GHz LTE MIMO operation in the smartphone. *Microw Opt Technl Lett*. 2016;58(1):174-181.
- [4] Al-Hadi AA, Ilvonen J, Valkonen R, Viikari V. Eight-element antenna array for diversity and mimo mobile terminal in LTE 3500 MHz band. *Microw Opt Technl Lett*. 2014;56(6):1323-1327.
- [5] Sharawi MS, Podilchak SK, Khan MU, Antar YM. Dual-frequency RDRA-based MIMO antenna system for wireless access points. *IET Microw Antennas Propag*. 2017;11(8):1174-1182.
- [6] Keyrouz S, Caratelli D. Dielectric resonator antennas: basic concepts, design guidelines, and recent developments at millimeter-wave frequencies. *Int J Antenn Propag*. 2016;2016:1-20.
- [7] Rashidian A, Aligodarz MT, Shafai L, Klymyshyn DM. On the matching of microstrip-fed dielectric resonator antennas. *IEEE Trans Antennas Propag*. 2013;61(10):5291-5296.
- [8] Zhang BH, Zhang JW, Liu CG, Wu Z. Investigation of microstrip-fed low-profile broadband circularly polarized rectangular dielectric resonator antennas. *Microw Opt Technl Lett*. 2017;59(11):2767-2772.
- [9] Shen B, Zhai WT, Zheng W. Ultrathin flexible graphene film: an excellent thermal conducting material with efficient EMI shielding. *AdvFunctMater*. 2014;24:4542-4548.
- [10] Sajal SZ and Braaten BD. A microstrip patch antenna manufactured with flexible graphene-based conducting material, 2015 I.E. International Symposium on Antennas and Propagation & USN-C/URSI National Radio Science Meeting; (2015), pp. 2415-2416.
- [11] Li J et al. Radiation-pattern-reconfigurable graphene leaky-wave antenna at terahertz band based on dielectric grating structure. *IEEE Antennas Wireless Propag Papers*. 2017; 16:1771-1775.
- [12] Hosseininejad SE, Komjani N. Waveguide-fed tunable terahertz antenna based on hybrid graphene-metal structure. *IEEE Trans. Antennas Propag*. 2016;64(9):3787-3793.
- [13] Fuscaldo W, Burghignoli P, Baccarelli P, Galli A. Graphene Fabry-Perot cavity leaky-wave antennas: plasmonic versus non-plasmonic solutions. *IEEE Trans. Antennas Propag*. 2017;65(4): 1651-1660.
- [14] Lamminen A, Arapov K, de With G, et al. Graphene-flakes printed wideband elliptical dipole antenna for low-cost wireless communications applications. *IEEE Antennas Wireless Propag Papers*. 2017;16:1883-1886.
- [15] Alvarez C, Cheung R, Thompson J. Performance analysis of hybrid metal-graphene frequency reconfigurable antennas in the microwave regime. *IEEE Trans Antennas Propag*. 2017;65(4): 1558-1569.


- [16] Marcatili EAJ. Dielectric rectangular waveguide and directional coupler for integrated optics. *Bell Syst Tech J.* 1969;48(7): 2071-2102.

**How to cite this article:** Xia W, Zhang B, Zhou W, et al. Rectangular dielectric resonator antenna fed by offset tapered copper and graphene microstrip lines for 5G communications. *Microw Opt Technol Lett.* 2018;60:2540–2547. <https://doi.org/10.1002/mop.31373>

Received: 5 March 2018

DOI: 10.1002/mop.31372

# A hybrid shielding structure for reduction of the leakage magnetic field in wireless power transfer system

Jongchan Kim<sup>1</sup> | Minjoo Jeong<sup>2</sup>  | Icpyo Hong<sup>3</sup> | Seungyeop Rhee<sup>4</sup> | Inkui Cho<sup>5</sup> | Nam Kim<sup>2</sup>

<sup>1</sup>Korea Communications Agency, 760, Bitgaram-ro, Naju-si, Jeollanam-do 58324, Republic of Korea

<sup>2</sup>Department of Information & Communication Engineering, Chungbuk National University, 1, Chungdae-ro, Seowon-gu, cheongju-si, Chungcheongbuk-do 28644, Republic of Korea.

<sup>3</sup>Department of Information & Communication Engineering, Kongju National University, 1223-24, Cheonan-daero, Seobuk-gu, Cheonan-si, Chungcheongnam-do 31080, Republic of Korea.

<sup>4</sup>Department of Electronic Communication Engineering, Chonnam National University, 50, Daehak-ro, Yeosu-si, Jeollanam-do 59626, Republic of Korea.

<sup>5</sup>Radio Technology Research Department, Electronics and Telecommunications Research Institute, 218, Gajeong-ro, Yuseong-gu, Daejeon 34129, Republic of Korea.

## Correspondence

Nam Kim

Department of Information & Communication Engineering, Chungbuk National University, 1, Chungdae-ro, Seowon-gu, cheongju-si, Chungcheongbuk-do 28644, Republic of Korea.

Email: namkim@chungbuk.ac.kr

## Abstract

In this paper, we propose a hybrid shielding structure for the reduction of the leakage magnetic field in the wireless power transfer (WPT) system operating at 175 kHz. This structure consists of ferrite slab staked on the

aluminum plate. The improvement in the magnetic field reduction is achieved, while minimizing the power transfer loss by optimizing the design parameters. The power transfer efficiency and leakage magnetic field are analyzed and verified through simulation and experiment. The experimental results show 77% power transfer efficiency with proposed structure, while the normalized leakage magnetic field strength was reduced up to 80% compared with the conventional shielding structures.

## KEYWORDS

hybrid shielding structure, magnetic field shielding, wireless power transfer

## 1 | INTRODUCTION

Recently, wireless power transfer (WPT) technology has been used in a variety of applications, including mobile phones, home appliances, and electric vehicles.<sup>1–3</sup> WPT technology has several advantages, such as an operation without physical contact and in wet and dusty environments.<sup>4</sup> However, WPT system causes some problems, including increased human exposure to electromagnetic fields (EMFs) and electromagnetic interference with other electrical devices due to accompanied relatively intensive EMFs. To solve these EMF-related problems, various shielding methods have been studied, focusing on shielding materials and structures.<sup>4–6</sup> Efficiency is the most important performance parameter for WPT systems. A coil structure, matching circuit, and magnetic shielding structure are considered to improve power transfer efficiency.<sup>7–10</sup> In previous research, the leakage magnetic field was reduced either by using magnetic material to adjust the magnetic flux path or by using conductive material to cancel the magnetic field.<sup>11,12</sup> This paper proposes a modified shielding structure with the ferrite and aluminum that can reduce the leakage magnetic field while maintaining high-power transfer efficiency.

## 2 | WPT COIL SYSTEM

Figure 1 shows the coil model used in proposed WPT system, which is designed using the Qi compliant A10 coil model developed by the Wireless Power Consortium.<sup>13</sup> The coil geometry consists of two layers with 10 turns. The inner radius of coils is 10.8 mm, and the outer radius is 20.92 mm. Input power is 200 mW at an operating frequency of 175 kHz. Figure 2 shows the conventional shielding methods applied to the transmitting (Tx) coil to reduce the leakage magnetic field generated from the WPT coil. Figure 2Aa shows the WPT system using the ferrite. The ferrite has